scientific reports

Check for updates

OPEN

Analysis of the CO_2 adsorption on AC: experimentation and statistical studies

Souhail.M. Bouzgarrou[1]✉, Khouloud Guettiti[2], Amin Naifar[3,4], Fatma Aouaini[5], Afzal Husain Khan[1], Rym Hassani[6] & Gamal A. Abdelhamed Saad[1]

The rising concentration of atmospheric CO_2 is a major driver of climate change, necessitating the development of efficient carbon capture technologies. This study quantitatively investigates the surface buildup and multilayer adsorption behavior of CO_2 on activated carbon (AC) using a probabilistic modeling framework in conjunction with adsorption experiments. Key parameters analyzed include the number of adsorption layers, adhesion energy (ΔEa), internal energy (Eint), and void density (DM). Results reveal that CO_2 adsorption on AC forms three to four distinct layers under optimal pressure and temperature conditions, with elevated temperatures reducing the number of layers due to increased interaction energy. The process is characterized as exothermic physisorption (ΔEa: 23.08–23.78 kJ/mol) with no evidence of chemical bonding. Multilayer adsorption effectively compensates for AC's high density of active sites, thereby enhancing CO_2 capture efficiency. These insights advance the understanding of CO_2 sorption mechanisms on heterogeneous surfaces and guide the design of more thermally stable and efficient carbon capture materials.

Keywords Multilayer scenario, Activated Carbon, CO_2, Gas efflux, Probabilistic mechanics, Modeling

One of the main causes of the observed acceleration in global warming is the significant increase in greenhouse gas concentrations over the past century, especially carbon dioxide (CO_2). The concentrations of greenhouse gases in the atmosphere are at their highest points in recorded history[1]. The biggest issues affecting greenhouse gases and global warming are supposedly CO2 storage and capture. Measurements show that atmospheric CO_2 concentrations have risen to an unprecedented level, from roughly 280 parts per million (ppm) before the industrial period to above 420 ppm in recent years[1,2]. This rise in CO2 concentration has intensified worldwide due to industrial and anthropogenic activities, particularly combustion, the burning of fossil fuels, and the combustion of organic matter to generate energy[3]. Whereas incomplete combustion of hydrocarbons in industrial factories, particularly from electrical substations, resulted in the emission of 23% of atmospheric acid gas[4]. It is suggested that fossil fuels and hydrocarbons are the main sources of energy generation, and estimated that this number will ascent by about 30% by 2035. In order to address this issue, studies have been conducted to identify highly adsorbent materials, particularly CO2, and to optimise adsorption by using statistical models that take into account physico-chemical factors.

Several research studies now prioritize regulating CO_2 industry emissions[5,6]. Regardless of the extensive consumption of non-renewable energy sources, it is critical to improve new knowledge that will allow us to reduce greenhouse gas emissions. Many scientists are interested in CO_2 adsorption on porous sorbents because it protects the environment, and many approaches to separate CO_2 from exhaust gases rely on adsorption capacity[5–7].

There are important uses of activated carbon (AC) in water and wastewater treatment too, such as eliminating heavy metals, pesticides, and groundwater remediation. On the other hand, AC is considered a good material for purifying air and gas too, it captures odors, harmful gases, and volatile organic compounds (VOCs) (in industrial emissions or respirators). For instance, gases like CO_2, H_2S, and CH_4 are efficiently captured and

[1]Civil and Architectural Engineering Department, College of Engineering and Computer Sciences, Jazan University, P.O Box 706, 45142 Jazan, Saudi Arabia. [2]Laboratory of Mechanics, Materials and Processes (LR99ES05), University of Tunis, ENSIT, 1008 Montfleury, Tunisia. [3]Preparatory Institute for Engineering Studies of Kairouan, (I.P.E.I.K), University of Kairouan, Kairouan, Tunisia. [4]Laboratory of Chemistry, Materials and Modelling (LR24ES02), Department of Physics, University of Kairouan, Kairouan, Tunisia. [5]Department of Physics, Faculty of Science, University of Monastir, BP56, 5000 Monastir, Tunisia. [6]Chemistry Department, Center for Environmental and Nature Research, Jazan University, P.O Box 114, Jazan, Saudi Arabia. ✉email: sbouzgarrou@jazanu.edu.sa; s_bouzgarrou2002@yahoo.fr

adsorbed by microporous adsorbents[8,9]. On comparing two adsorbents for minimizing atmospheric pollutants reveals that AC has physical and chemical features more efficient of adsorbing higher quantities of gas than molecular sieves[3].

Among various adsorbents, the AC used in this study is powdered activated carbon (PAC), whose pore structure plays a major role in adsorption. The AC micropores with dimensions smaller than 2 nm enable the adsorption of tiny molecules, including gases and volatile organic compounds, whereas mesopores, which range in size from 2 to 50 nm, improve micropore accessibility and allow larger molecules to slip through[10]. The large surface area of AC make it a popular adsorbent, which can range from 600 to 1500 m^2/g[11]. Since that indicate the number of adsorption sites available for the entrapment of assorted organic/inorganic matter, AC's surface area is paramount to its adhesion properties[11]. One more decisive factor is AC's pore size distribution. Pore sizes between 8.9 and 27.9 Å are particularly important for adhesion processes, with larger pores allowing for more retention due to reduced wall effects[12]. The adsorptive efficiency of AC is also significantly dependent on its mineral composition. The main component of ACs is carbon, and they have a higher degree of porosity and a enormous internal surface area[13].

The efficiency of AC produced from biomass for CO_2 adsorption has been shown in recent studies. Agricultural waste, such as coconut husks and olive leftovers, can be utilized to make ACs. Even different types of AC are being used in various industries. These industrial absorbents are frequently successful when the adsorption cycle is properly designed and the adsorbents are chosen under ideal operating conditions[14]. For several gas molecules, these properties promote a greater adsorption capacity and a favorable kinetic selection[15]. Despite being suitable for this purpose, AC's other benefits include its capacity to both adsorb and desorb molecules. Usually, carbonization and chemical or physical activation methods are used to produce ACs from biomass. Another method to extract CO_2 is temperature–pressure cycling adhesion. Such a technique may be applied to both gas desorption and adsorption (Jedli et al., 2017[16]). AC is a practical porous design for adhesion along with gas confinement. AC substrates are synthesized from biomass (gelatin and starch) via chemical activation, showing a higher surface areas (1636–1957 $m^2\ g^{-1}$), while numerous nanoscale voids with pore sizes of around 1.95 nm[17].

To investigate the inherent features of ACs, methods such as scanning electron microscopy (SEM), nitrogen adsorption–desorption (BET), and X-ray diffraction (XRD) are frequently used. It also contributes to analyzing reactive specific surface area and pore distribution[18]. For adsorption isotherms and statistical models, such as the Langmuir model and the response surface approach, are essential for maximizing the adsorption procedure and enhancing the efficiency of adsorbent materials. The design and optimization of CO2 capture systems have been improved through enhanced modeling techniques, which have further enhanced our understanding of adsorption isotherms and kinetics[19]. The adopted statistical framework is novel for describing the CO2 adhesion isotherm mechanism on the exterior of the AC[15]. A recent research evaluated the adsorption performance of CO2 on AC under various pressures and temperatures, confirming the importance of experimental conditions on the adsorption efficiency[20]. In addition, energy efficiency is crucial throughout the adsorption and desorption processes for AC. Whereas intermolecular interactions brought on by electrostatic interactions are known as van der Waals forces. These are minor, readily destroyable implicit forces (Michel et al., 2006)[21].

In our work, we examine CO_2 surface accumulation on AC extensively. To understand the mechanisms of CO_2 adsorption at the molecular level, statistical models are essential for researching the adsorption of CO_2 on materials such as AC. Comprehend the interaction with adsorbent surfaces, as the models allow the quantification of the maximum CO_2 adsorption capacity for material property optimization. Adsorption isotherms were established at four different operating temperatures in order to examine the isothermal behavior of CO_2 adsorption within the microporous structure of AC. This study's methodological component used a number of physical models developed to clarify the microscopic mechanisms of CO_2 adsorption on AC. A thorough description of adsorption phenomena under various thermodynamic conditions was made possible by the theoretical framework, which was founded on statistical physics, more especially the grand canonical ensemble. A thorough grasp in a variety of thermal environments was made possible by this method, which made it easier to fit experimental isotherm data at four different temperatures: 26, 43, 51, and 62.5 °C.

The adjusted findings are deployed to AC and CO_2 accumulation, followed by acquiring insights at the molecular level. From fitting, extracted pH, temperature, and salinity were correlated to ascertain the impact of some of the adsorbent's intrinsic features. Furthermore, the temperature variations provided significant data on pore dimensions and adsorbent mass. As a result, this paper advances our understanding of how gaseous CO_2 adsorbs onto AC. The modified outcomes have been directed to elucidate the CO_2/AC system by providing a deep physical discussion. The influence of certain inherent features of the adsorbent was ascertained by comparing the realized physicochemical parameters. Additionally, the temperature at which the AC was placed revealed crucial details about the size of its pores. Our study thus provides new insights into CO_2 gas retention near AC sites.

Technical section and methodology

Section on technology and experiments

The activated carbon (AC) used in this study was purchased from chemviron kuraray company, in Feluy located in the province of Hainaut, Belgium. According to the supplier, the AC was derived from a high-quality bituminous coal. the outer diameter length was approximately 10–50 µm and purity of >95%. Chemviron (AC) is made from coal using a number of steps that are intended to produce a porous, high-surface-area material. First, the bituminous coal with a high carbon content is heated to temperatures of about 750 °C in an inert atmosphere, which drives off moisture and volatile compounds, turning it into char. Next, it is activated, which en-tails exposing it to oxidizing gases at high temperatures of about 1000°C. This step increases the surface area, affect density and creates a network of pores. Finally, the sample was washed with distilled water until neutral pH and

Adsorbents	Specific surface (m^2. g^{-1})	Pore size (nm)	Internal porosity
Activated Charcoal	200 to 400	1.0 to 4.0	0.4 to 0.8
Molecular Sieve	300 to 600	0.3 to 0.8	0.35 to 0.5
Zeolites	500 to 800	0.3 to 0.8	0.3 to 0.4

Table 1. Comparison of specific adsorbents' physical characteristics[23]

Adsorbents	Carbon	Oxygen	Hydrogen	Nitrogen	Sulfur
AC	56.00	35.9	7.60	0.35	0.1

Table 2. Atomic arrangement of AC substrate.

Adsorbents	SiO_2	Al_2O_3	CaO	Fe_2O_3	Na_2O	K_2O	MgO	$CaCO_3$
AC	**45.23**	**15.45**	**10.22**	**11.95**	**4.3**	**4.2**	**6.8**	**0.5**
El Hicha Clay	49.22	13.75	9.34	6.08	1.16	0.56	2.22	-
Carbon Molecular Sieve	38.54	26.42	0.636	1.74	14.8	0.07	0.083	-
Source: Activated Carbon (AC); El Hicha Clay; Molecular Sieve								

Table 3. The chemical makeup of the various capture adsorbents (Bonnard et al., 2005)[25].

dried at 109 °C temperature for about 18 hours. The AC had a surface area of 879 m^2/g and an average pore size is 0.540 cm^3/g The characterization of activated carbon mostly relies on sample preparation and sampling; the majority of measuring techniques necessitate meticulous sample preparation, which involves heating the sample under precise conditions to eliminate adsorbed humidity and other gases[22]. Since it dictates the ACs' moisture content, catalytic characteristics, and acid–base nature, surface chemistry has a major impact on their adsorption capacity[11]. As a whole, the characterization of AC entails determining its mineral composition, surface area, and void dimension variation, all of which are critical components of its retention attributes.

Table 1 compare the primary physical characteristics of activated charcoal, molecular sieves, and zeolites. The components found within the surface of the AC substrate are detailed in Table 2. Activated charcoal is very effective for odor control and broad-spectrum adsorption (large specific surface area, diverse pores).

The Brunauer–Emmett–Teller (BET) method was used to determine the specific surface area from the N2 isotherm. The Barrett–Joyner–Halenda (BJH) method was used to determine the mesopore size distribution; the sample is made up of tiny particles, and the specific surface area, BET, is 879 m^2/g. The total pore volume is 0.540 cm^3/g. Because of their large surface area, quick adsorption kinetics, and efficiency in eliminating pollutants in suspension, these ACs are mostly employed in water treatment procedures[24].

Zeolites are employed in selective gas adsorption, such as the removal of ammonia, ion exchange, and catalysis. Because of their stiff pores, molecular sieves are perfect for size-selective separation (drying gases, CO_2 capture)[23,25]. The mass percentages of chemical elements composing the adsorbents studied in this work are determined by X-ray fluorescence. First, the sample is treated to X-ray radiation to get the atoms in the material excited. When the excited atoms go back to their ground state, they emit secondary X-rays. The elements present and their concentrations are then determined by detecting and analysing these released X-rays. (Table 2 and Table 3).

Carbonization and activation procedures are used to produce activated charcoal. Steam or CO_2 can be used for physical activation, while acids or alkalis can be used for chemical activation. Intrinsic attributes of the AC, including void dimension repartition and adsorption capacity, are greatly influenced by the choice of precursor material (such as wood, coal, or coconut shells).

Figure 1 displays the sample's SEM image. Several types of randomly scattered holes exist on its heterogeneous surface. Furthermore, it is evident that the AC has a porous structure. The pores are easily discernible and come in a wide range of sizes. Some measurement indications are shown by the blue lines, which show the diameters of particular holes or surface characteristics on the material in micrometers (μm). The diameter of these pores is shown by the numbers adjacent to the lines. By matching the size of a pore or structural feature, these measurements help to offer information on the material's porosity and surface characteristics. Comprehending these measures can aid in assessing the material's suitability for specific applications, such figuring out how effectively it adsorbs in catalysts or filters.

The activated carbon type chemviron, used in its as-received state, was characterized using a Thermo Fisher FEI Q250 scanning electron microscope with an accelerating voltage of 10–15 kV, at magnifications of 10 μm.

The mass (%) of atoms present in the AC volume could be established thanks to the X-ray fluorescence. The carbon amount, as well as the outcomes of AC's analysis, are provided in Table 2. The sample's essential composition was around 35.9% oxygen (O), 56.00% carbon (C), 7.6% hydrogen (H), 0.1% sulfur (S), and 0.35% nitrogen (N). AC has a high concentration of carbon and oxygen due to volatile molecules that are present during the carbonization process (see Table 3).

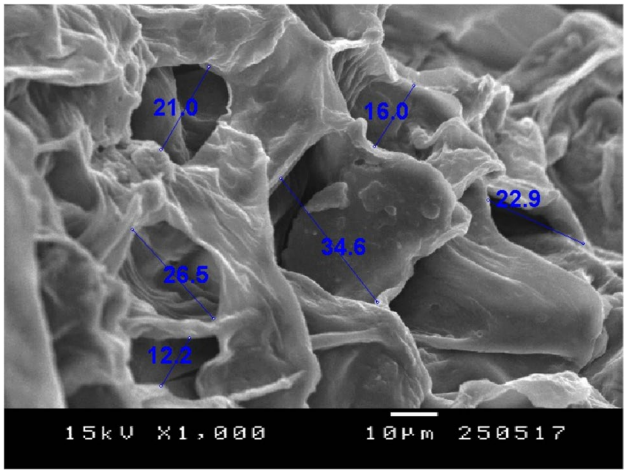

Fig. 1. SEM images of AC.

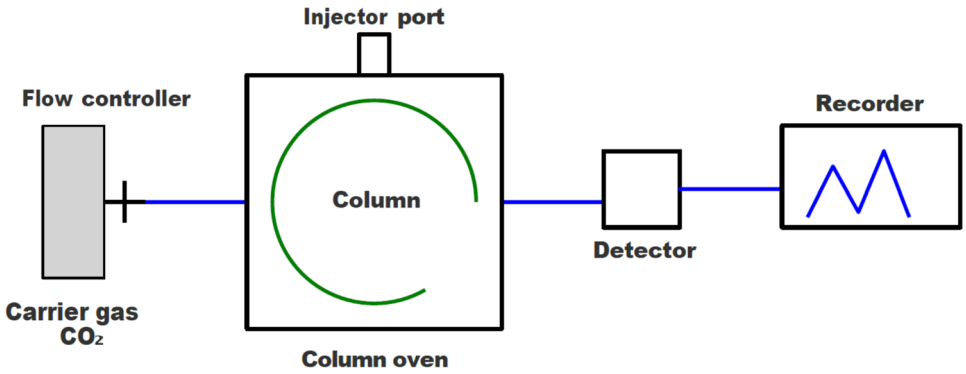

Fig. 2. Layout of the flowchart set-up[6].

The graphite crystallites that make up AC's whole surface are smaller in size, which might result in internal structure disorder or expansion and a higher accessible surface. It is observed that the texture of AC contains ultramicroporous fine powders. The specific surface area increases with decreasing crystallinity[26].

Experimental method

This study examines CO_2 surface accumulation using an "IGC 10 M series" chromatograph on a 10 Å MS, as shown in Fig. 2. Understanding the features of a substance's outer layer and internal structure is crucial and is a sensitive and adaptable analytical method for physicochemical characteristics[6]. Inverse Gas Chromatography (IGC) with high-purity CO_2 (99.99%) was used as the adsorbate gas, while all other reagents were of analytical grade (≥ 99% purity) to offer a distinctive approach to achieve this. This method adapts standard gas chromatography, switching the typical relationship between the fixed and moving components to enable the study of a sample of interest. After filling with a mass of adsorbent, the adsorption column was conditioned under a flowing stream of carrier gas and heated overnight at a temperature of approximately 120 °C to remove all residual moisture. The most significant difference between these samples is the particle size and the difference in external surface area.

The three most significant characteristics are the exterior surface, particle size, and mineralogical content. The gas is directly injected into the chromatograph using the flow control valve once the experimental apparatus has reached room temperature the next day. Figure 2 displays a schematic graph of the experimental construction[27]. To remove any residual moisture, the retention set-up chromatography is subjected to heating at around 120 °C for the remainder of the night after the adsorbent mass has been filled. For every injection test, the approach a particular amount of gas within the column at the steady-state thermodynamic condition[27]. CO_2 can be adsorbed at a range of temperatures, pressures, and flow rates. By altering two parameters, the pressure and stream flow are simultaneously measured for each CO_2 input.

The gas-phase chromatographic method provides the foundation for the technique used to calculate the CO_2 adsorption isotherms on various adsorbents. Under a given load pressure, a specified quantity of CO_2 is accumulated to allow for chromatographic elution. Based on the injection temperature and discharge value, a peak-shaped electrical signal is generated and recorded on a recorder's paper[5,6].

Results and discussion

CO_2/AC isothermal profiles were inspected via three fitting frameworks: a single-layer model (Model 1), a two-layer scenario with two distinct energies (Model 2), and a multilayer model with saturation (Model 3). The adopted scenarios are defined based on the grand canonical distribution approach from probabilistic formalism[3,28–31]. In addition, Table 4 explains the physical interpretation of the three models:

Model 1: Describes monolayer adsorption where each adsorption site can retain only one layer of n_{CO_2} molecule.

Model 2: Represents two-layer adsorption with two energies, simulating adsorption at moderate pressures of two layers.

Model 3: Accounts for the multilayer adsorption with saturation, where multiple layers of CO_2 molecules accumulate, particularly at higher pressures and lower temperatures-providing a more realistic view of surface saturation and adsorption dynamics.

In Table 4, n represents the number of molecules of CO_2 linked per AC site, D_M, is the density of receptor site, $P_{1/2}$, P_1, and P_2 represent the pressure at half saturation (mmHg), and the N_2 is the number of layers formed on the AC surface. The tested scenarios of the three models are shown in Table 4.

Two coefficients are used as indicators of the overall goodness of the fit. The first is R^2, which is known as the coefficient of determination. Its expression is given by Eq. 4:

$$R^2 = 1 - \left[1 - \left(\frac{\sum_i^n (Q_{i\,\exp} - \overline{Q_{i\,\exp}})^2 - \sum_i^n (Q_{i\,\exp} - Q_{i\ \mathrm{mod}\ el})^2}{\sum_i^n (Q_{i\,\exp} - \overline{Q_{i\,\exp}})^2}\right)\right]\left[\frac{n_p - 1}{n_p - p}\right] \tag{4}$$

With $Q_{i\ \mathrm{mod}\ el}$ as the anchored variable whose corresponding numerical data are assigned to the model, $Q_{i\,\exp}$ as the variable obtained from the experiment, $\overline{Q_{i\,\exp}}$ as the average test result, np as the set of test points and p as the indispensable matching number. The second coefficient is the residual root mean square error (RMSE), which is also referred to as the estimated standard error of the regression. Thus, for a quantity p of modifiable parameters, the calculated standard error is expressed as:

$$RMSE = \sqrt{\frac{RSS}{m' - p}} \tag{5}$$

where RSS is the residual sum of squares $RSS = \sum_{j=1}^{m'} (Q_{j,cal} - Q_{j,exp})^2$. Q_{jcal} and Q_{jexp} represent the calculated and experimental values of the adsorbed amount, respectively, while m′ denotes the count of experimental data. It is recognized that when the absorption isotherms closely align with the selected model, the determination coefficient R^2 approaches 1, and the RMSE values are nearly zero. The various values of R^2 and RMSE are presented in Table 5. Thus, Model 3 shows the highest R^2 values and the lowest RMSE values.

Understanding the interaction between adsorbate molecules and the adsorbent requires studying adsorption isotherms, as shown in Fig. 3. Researching adsorption isotherms is necessary to measure adsorption capacity; thereafter, one can determine how much adsorbate can be adsorbed by a certain volume of adsorbent under particular variables like temperature, pressure, and concentration. Conversely, that would enable numerical model development by predicting adsorption behavior.

The plot of the curve ΔH_{ads} as a function of the adsorbed quantity q is shown in Fig. 4. The existence of several extremum points in the plot of adsorption heat against adsorption quantity (Fig. 4) highlights the heterogeneous characteristics of the AC surface along with the multilayer adsorption process. These extrema result from shifts

Model	Q_a (g/g)
Monolayer (Model 1)	$Q_a = \frac{n.D_M}{\left(1+\left(\frac{P_{1/2}}{P}\right)\right)}$ **(1)**
Two layer with two energies (Model 2)	$Q_a = n.D_M \frac{\left(\frac{P}{P_1}\right)^n + 2.\left(\frac{P}{P_2}\right)^{2n}}{1+\left(\frac{P}{P_1}\right)^n + \left(\frac{P}{P_2}\right)^{2n}}$ **(2)**
Multilayer model with saturation (Model 3)	$Q_a = n.D_M.\frac{\frac{-2(\frac{P}{P_1})^{2n}}{(1-(\frac{P}{P_1})^n)} + \frac{(\frac{P}{P_1})^n(1-(\frac{P}{P_1})^{2n})}{(1-(\frac{P}{P_1})^n)^2} + 2\frac{(\frac{P}{P_1})^n(\frac{P}{P_2})^n(1-(\frac{P}{P_2})^{nN_2})}{(1-(\frac{P}{P_2})^n)} - \frac{(\frac{P}{P_1})^n(\frac{P}{P_2})^n(\frac{P}{P_2})^{nN_2}N_2(1-(\frac{P}{P_2})^n)}{(1-(\frac{P}{P_2})^n)} + \frac{(\frac{P}{P_1})^n(\frac{P}{P_2})^{2n}(1-(\frac{P}{P_2})^{nN_2})}{(1-(\frac{P}{P_2})^n)^2}}{\frac{(1-(\frac{P}{P_1})^{2n})}{(1-(\frac{P}{P_2})^n)} + \frac{(\frac{P}{P_1})^n(\frac{P}{P_2})^n(1-(\frac{P}{P_2})^{nN_2})}{(1-(\frac{P}{P_2})^n)}}$ **(3)**

Table 4. Tested scenarios and corresponding formulas.

CO_2/AC						
Model	Model 1		Model 2		Model 3	
T (°C)	R^2	RMSE	R^2	RMSE	R^2	RMSE
26	0.99963	1.1421×10^{-4}	0.99885	5.6610×10^{-4}	**0.99948**	$\mathbf{3.3908 \times 10^{-4}}$
43	0.99938	3.0414×10^{-4}	0.99924	3.1772×10^{-4}	**0.99941**	$\mathbf{2.4512 \times 10^{-4}}$
51	0.99966	9.4414×10^{-4}	0.99975	9.8661×10^{-4}	**0.99994**	$\mathbf{8.3345 \times 10^{-6}}$
62.5	99,961	3.4978×10^{-4}	0.99959	1.66451×10^{-4}	**0.99995**	$\mathbf{1.7187 \times 10^{-6}}$

Table 5. The R^2 value of the coefficient of determination and the residual root mean square error (RMSE) for the CO_2/AC system at various temperatures.

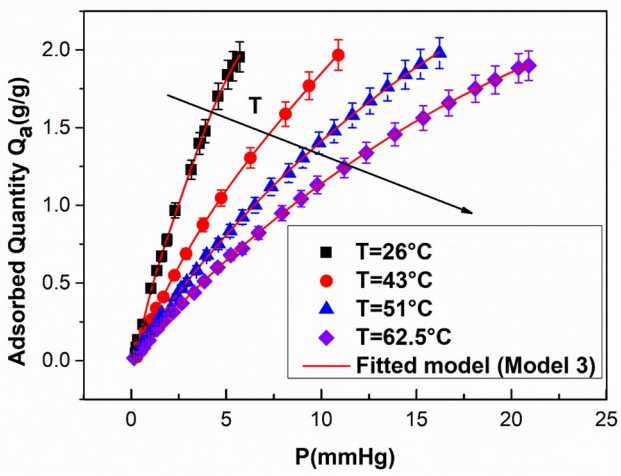

Fig. 3. Adjustment of isotherms of CO_2 on AC by the saturated multi-layered framework at different temperatures.

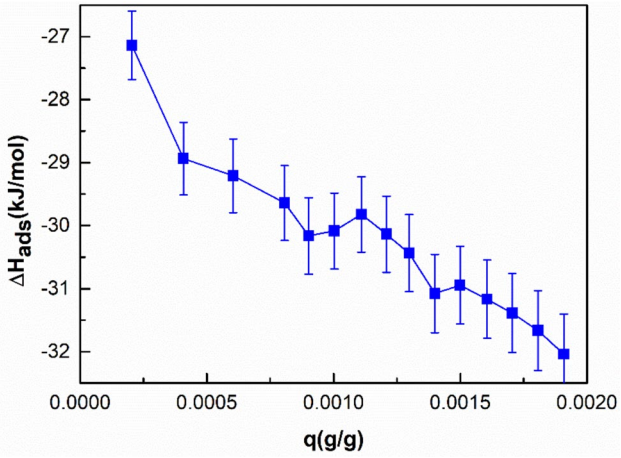

Fig. 4. Adsorption enthalpies of CO_2/AC.

between adsorption layers, where changes in binding energies happen due to varying interactions between CO_2 molecules and the surface, as well as previously adsorbed layers. At first, intense interactions take place at high-energy primary sites, then gradually weaker interactions happen as adsorption moves to secondary and tertiary layers. The adsorption heat values were determined using the Clausius–Clapeyron equation from isotherms collected at various temperatures. Nonlinear regression techniques were utilized for data fitting, accompanied by residual analysis to verify model reliability. The existence of duplicate measurements additionally confirmed the reliability of the recorded extrema. These methodological procedures validate that the characteristics seen in Fig. 4 are both physically significant and replicable.

CO_2- AC							
T(°C)	n	D_M	N_1	P_{ls1}(mmHg)	P_{ls2}(mmHg)	ΔE_1^a (kJ/mol)	ΔE_2^a (kJ/mol)
26	1.704	0.4726	2.3189	1.0589	4.5745	−26.715	−23.079
43	1.1653	0.8318	2.9652	5.5603	34.0734	−24.853	−20.093
51	1.0463	1.2084	2.0689	5.9643	22.8417	−25.928	−21.047
62.5	1.1263	0.9866	2.3340	4.8348	20.5574	−27.809	−23.780

Table 6. Different parameter values according to scenario 3.

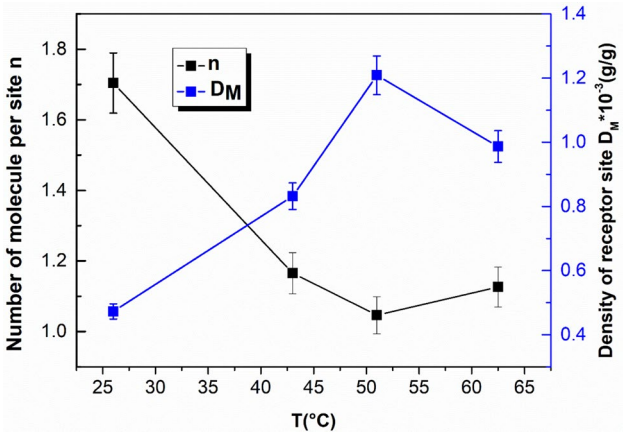

Fig. 5. Temperature impact on the evolution of n and D_M.

In Fig. 4, the variation of adsorption heat (ΔH_{ads}) with adsorption quantity (q) for CO_2 on AC. Multiple extremum points are observed, corresponding to transitions between adsorption layers and changes in interaction energies across heterogeneous binding sites. Data were processed using the Clausius–Clapeyron method and validated through nonlinear regression and replicate measurements. Compared to bibliographic data, the adsorption enthalpy estimates fall within the range of physical adsorption. As a result, the CO_2/AC combination is experiencing physical adsorption. Since the isosteric enthalpy values are negative, the CO_2 adsorption process on AC is exothermic.

It is also evident that when the amount adsorbed rises, the isosteric temperatures of adsorption fall. The adsorption of the initial molecules on the initial layers occurs on the regions of the surface that exhibit the highest interaction energies, which explains this. The subsequent molecules then adsorb, reducing the amount of heat emitted. The average isosteric heat of adsorption during CO_2 adsorption on AC-type AC is 30.2392 kJ/mol. The non-homogeneity of the surface and the intricacy of the AC's chemical makeup can both be used to explain the enthalpy variation.

Linking metrics exploration

Here, our focus is on deploying framework 3 to elucidate the CO_2 retention when approaching the selected substrate. This model provides valuable insights into the adsorption mechanism due to its well-defined physical significance. As shown in Table 4, all three adhesion models assume that a range of CO_2 entities can link to accessible voids. These theoretical models propose that CO_2 molecules are adsorbed either through identical receptor sites or self-contained binding points (D_M), with a density of these linking locations[28]. Also, all estimated values of the adjustment of CO_2 on the AC adsorbent surface via the multilayer model with saturation (Model 3) are investigated in Table 6.

Impact of thermal agitation on n and D_M

From Fig. 5, it is observed that n_{CO2} decreases with temperature. Additionally, n_{CO2} is greater than one, indicating the mean linked species per void. This suggests a multimolecular adhesion process of CO_2 on the AC adsorbent surface. All computed n_{CO2} values are presented in Table 5, showing that more than one CO_2 molecule can be bound per adsorption site following the multimolecular adsorption process. For instance, at a temperature of 43 °C, n_{CO2} bound per void spans approximately in the interval[3]. Specifically, the fraction of cavities occupied by one entity (y) and those occupied by two molecules ($1-y$) may be estimated using the formula: $y\times1+(1-y)\times2=1.1653$. Solving this equation reveals that a single molecule occupies 83% of the retention voids, while 16% are occupied by two molecules. It can be deduced that the trend of n_{CO2} signals that the linking phase is heat-driven and thermal motion significantly influences the grouping tendency of CO_2 on the adsorbent surface.

Figure 5 describes the thermal impact on D_M. The latter denotes the void occupancy density. It seems that D_M changes oppositely in response to heat elevation. Witnessed incrementation of D_M against molecular fluctuations is satisfactorily explained when focusing on the n_{CO2} pattern. When $n_{CO2\ is}$ reduced, remaining unoccupied voids for CO_2 are also reduced, thus inducing a visible growth in bounding point density. In physical terms, the detected incrementation of D_M acts as an obstruction to additional entities when approaching voids (D_M rises).

Total count of generated layers (N_C)

As stipulated N_C denotes the complete count of generated adsorbate entities adhesion layers ($N_C = 1 + N_1$) produced throughout the linking stage. Figure 6 illustrates the consequence of heat intensification in N_C. As shown in Fig. 6, the major outcomes provided state that N_C ranged from 3.06 to 3.96. This suggests that CO_2 adsorption occurred through the formation of three to nearly four layers, with the number of layers decreasing as the adsorption temperature increased. This decrease may be attributed to higher interaction energies. Although the count of reactive voids for CO_2 linking on the substrate's area increments, it is somewhat counterbalanced by the adhesion in various layers. Physically, our findings imply a drastic variation in retention efficiency within sorbents is influenced by their ability to form multilayers, which can mitigate the impact of factors that negatively affect CO_2 adhesion.

CO_2 uptake capacity at saturation (Q_{sat})

Physically, Q_{sat} expresses the largest quantity of CO_2 when linked to a specific void for a determined heat level. Q_{sat} value is derived immediately sourced from the MMS framework by extrapolating the system pattern under high-pressure circumstances. Such a metric is intrinsically linked to N_C, D_M, and n_{CO2}, reflecting the AC adsorbent's capacities for capturing CO_2. Formally, Q_{sat} is defined as: $Q_{sat} = n_{CO2} \times N_C \times D_M$.

Figure 7 highlights the major consequence of heating when CO_2 is linked to voids. It confirms that the retention capacity increases with temperature (endothermic aspect) while the heat seems to strongly impact the grouping behavior. Notably, the binding strength of CO_2 species onto AC's cavities is thermally activated, causing the Q_{sat} to reduce. To heat alteration, stereographic metrics (n_{CO2}, D_M, and N_C) confirm the obtained outcomes. As the temperature rises, the values of n_{CO2} and N_C decrease while D_M increases. The combined effect of these changes leads to an overall increase in uptake capacity with temperature. Among these metrics, D_M has the most significant consequence on Q_{sat}.

Exploration of the surface adhesion energy

When characterizing the retention aspect while gaining more insights regarding the involved forces for the CO_2/AC complex, the retention energy of bounded species to accessible voids was determined using the MMS scenario. According to the MMS formula, the two pressures at half-saturation (P_{ls1} and P_{ls2}) correspond to the two adhesion energies. $(-\Delta E_1^a)$ and $(-\Delta E_2^a)$ that can be determined by the following expressions, which in turn allow investigation of their relationship with temperature[19]:

$$-\Delta E_1^a = -R.T.\ln\left(\frac{P_{vs}}{P_{ls1}}\right) \tag{6}$$

$$-\Delta E_2^a = -R.T.\ln\left(\frac{P_{vs}}{P_{ls2}}\right) \tag{7}$$

where P_{vs} is the saturated vapor pressure of CO_2 for a specific temperature, while R is the gas constant (8.314×10^{-3} kJ.K^{-1}.mol^{-1}). Above the critical temperature (T_c) (approximately equal to 304 K for CO_2), Dubinin (1975) stated the experimental formula to compute the pseudo-vapor pressure values[3,32–34]:

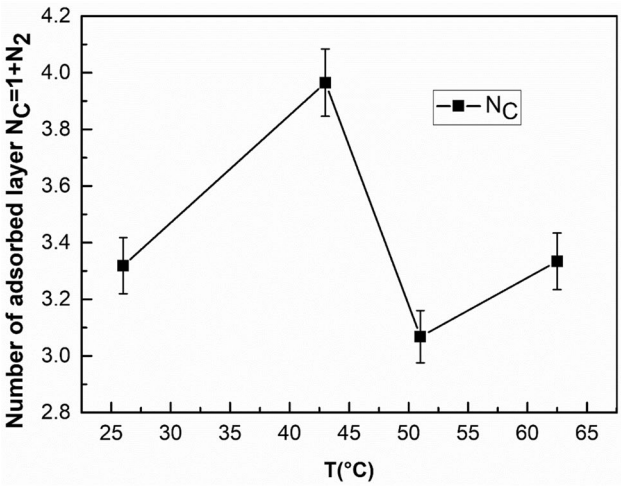

Fig. 6. Temperature impact on the evolution of the total number of layers N_C.

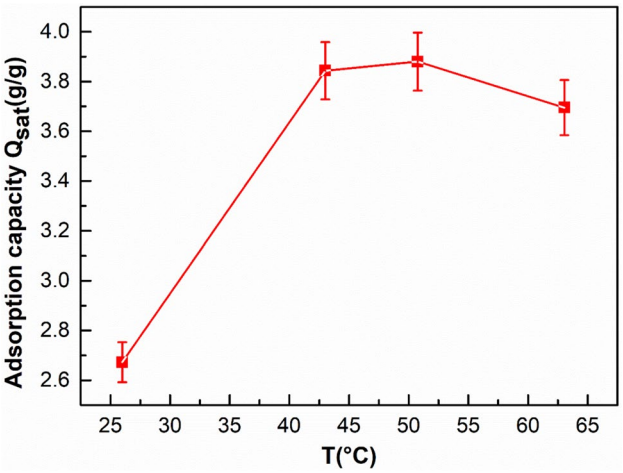

Fig. 7. Temperature impact on saturation adsorption capacity (Q_{sat}).

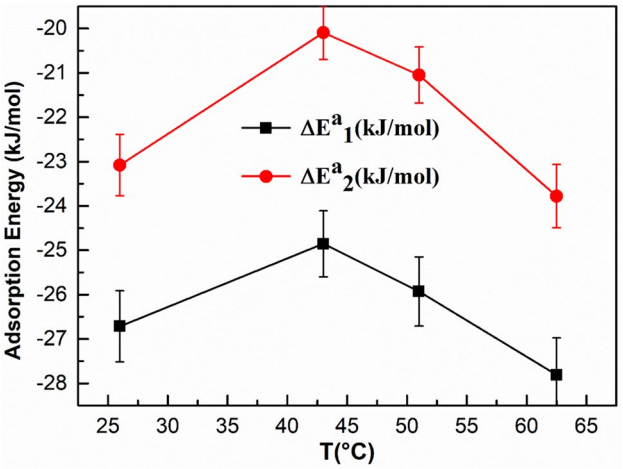

Fig. 8. Adsorption energies $(-\Delta E_1^a)$ and $(-\Delta E_2^a)$ evolution at different temperatures.

$$P_{vs} = P_C \left(\frac{T}{T_c}\right)^2 \tag{8}$$

where P_c represents the CO_2 critical pressure.

In physical terms, $(-\Delta E_1^a)$ resumes the energetic strength when dealing with CO_2-AC's voids while $(-\Delta E_2^a)$ distinguishes the CO_2-CO_2 connections regarding the progressive layers. The first term is bigger than the second one. This is attributed to the low-intensity forces emerging between the adsorbate and the adsorbate. All computed adhesion energies are < 35 kJ.mol^{-1}. This is indicative of the absence of covalent bounds (physisorption). In this case, van der Waals and London dispersion forces are the main drivers of CO_2 linking. Additionally, the negative values of the adhesion energies confirm the exothermicity of the binding mechanism.

Figure 8 illustrates the consequence of heating on the computed $(-\Delta E_1^a$ and $-\Delta E_2^a)$. Obviously, with hotter conditions, these two energetic quantities significantly rise with a visible pattern within [26–62.5 °C]. This tendency is justified by the expansion of available cavities as the experimental conditions become hotter. As a result, it elevates the mean energy of free voids. Primarily, CO_2 species link to voids with stronger affinities (stronger adhesion energies). Once these high-affinity sites are engaged, remaining species tend to bind onto lower-energy voids, whose linking energy subsequently increases.

Total internal energy E_{int}

Our numerical exploration is completed by inspection of internal energy: E_{int}. In this context, the focus is primarily on mutually shared forces that govern species[3,29–31,35]. Such an important quantity surrounds every type of power within the studied complex and explicitly represents the retention of energy. In our system, species are moving in a gaseous phase. The internal energy of free adsorbate molecules is given by[36]:

$$E_{\text{int}} = -\frac{\partial \ln(Z_{gc})}{\partial \beta} + \frac{\mu}{\beta}\left(\frac{\partial \ln(Z_{gc})}{\partial \mu}\right) \tag{9}$$

Figure 9 shows that the interaction energy E_{int} for CO_2 adsorption on AC is negative throughout the temperature range, confirming the exothermic nature of the process. The nonlinear trend arises because, although adsorption remains exothermic, the magnitude of E_{int} decrease as temperature increase. This reflects that higher thermal agitation at elevated temperatures reduces the binding strength of CO_2 molecules to the adsorbent surface, making adsorption less energetically favorable. Furthermore, the reduction in E_{int} with increasing pressure suggests that additional CO_2 molecules are more easily accommodated at receptor sites, but this effect is modulated by temperature-dependent changes in molecular mobility and pore accessibility. In summary, the nonlinear behavior results from the competing influences of thermal energy-promoting desorption-and adsorption forces-favoring molecule retention-combined with pressure effects that impact molecular packing and site occupation. This nuanced interplay leads to the observed variation in adsorption interaction energy with temperature.

The entropy of adsorption (S_a)

The entropy information is essential for defining the behavior of adsorbed molecules. It measures the movement of gas molecules (CO_2) regarding the receptor sites located on the surface of the AC-based adsorbent. In the field of statistical thermodynamics, adsorption entropy is described as a thermodynamic function that quantifies the disorder within the system on a microscopic scale. The entire system is made up of adsorbate molecules that interact with the surface of the adsorbent. The formula for the adsorption entropy (Sa) can be expressed as: (Eq. (6))[3,29–31]:

$$\frac{S_a}{k_B} = Ln(Z_{gc}) - \beta\frac{\partial Ln(Z_{gc})}{\partial \beta} \tag{10}$$

By employing the expression for the grand canonical function, Z_{gc}, in the multilayer model, to obtain the equation for the adsorption entropy. Taking into account entropy provides insights into the degree of disorder and randomness exhibited by the gas molecules during the adsorption process. Figure 10 illustrates how entropy varies with pressure at different temperatures for CO_2 adsorbed on the AC-based material. At low pressures, entropy increases, reflecting greater disorder as CO_2 molecules interact freely with a wide range of accessible receptor sites. This initial rise corresponds to the dynamic occupation of heterogeneous, high-energy adsorption sites. However, the trend becomes non-monotonic at intermediate pressures, as indicated by arrows in the figure. These fluctuations are attributed to the transition from monolayer to multilayer adsorption and the reorganization of adsorbed molecules into more ordered arrangements. As pressure continues to increase and the adsorbent near saturation, a marked decrease in entropy is observed. This decline results from the reduced availability of free adsorption sites and the confinement of CO_2 molecules, which limits their configurational freedom and leads to a more structured, less disordered system. The interplay between surface heterogeneity, multilayer formation, and temperature effects accounts for the observed non-monotonic entropy behavior.

Conclusion

In order to elucidate the adsorption mechanisms of CO_2 on AC, this study employed statistical physics modelling, revealing crucial information regarding the molecular-scale interactions that propel the process. The most suitable model was the multilayer framework with saturation, which showed that non-covalent interactions—mainly fuelled by London dispersion forces—are responsible for CO_2 retention within the exothermic energy

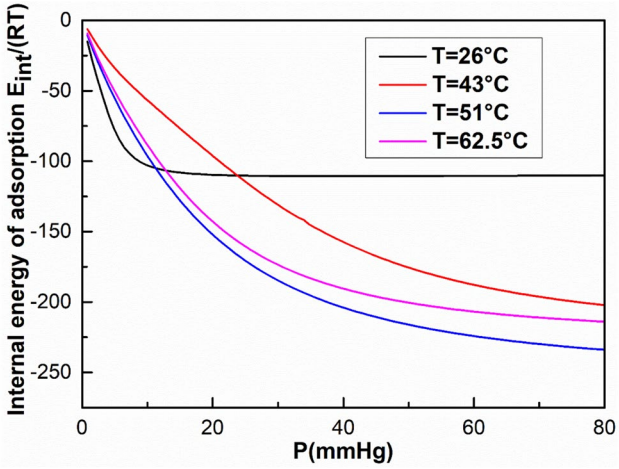

Fig. 9. Evolution of rapport (Eint/(RT)) against pressure at various temperature values.

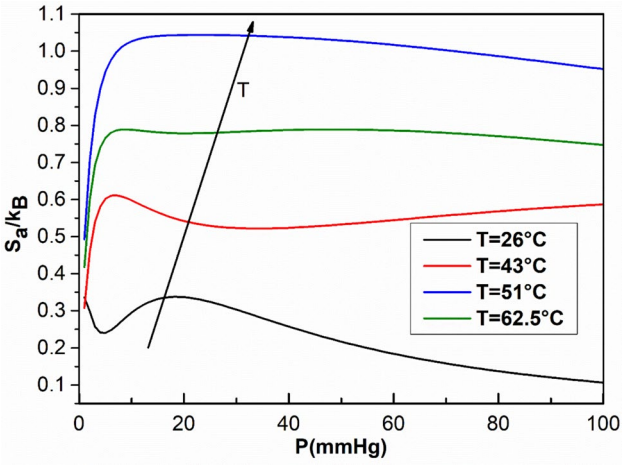

Fig. 10. Evolution of (Sa/kB) against pressure at various temperature values.

range of 23.079–23.780 kJ·mol^{-1}. Importantly, three to four layers were formed during adsorption, and as thermal agitation increased, the layers' density decreased.

These results have important implications for carbon capture technologies, as they elucidate the thermodynamic and mechanistic behavior of CO_2 adsorption on porous materials. The findings align with the study's aim of enhancing adsorption processes by measuring how temperature and pressure influence cavity occupancy and saturation capacity. This study strengthens the scientific basis for raising CO_2 capture efficiency, which is crucial considering the urgent necessity to solve climate change. Future studies should look at scalable uses of these discoveries, particularly in industrial adsorption systems, to enhance techniques for sequestering greenhouse gases.

Data availability

Data will be made available on request by Dr. Souhail. M Bouzgarrou, Email id: sbouzgarrou@jazanu.edu.sa.

Received: 12 March 2025; Accepted: 29 September 2025
Published online: 04 November 2025

References

1. Summerhayes, C. P. et al. The future extent of the Anthropocene epoch: A synthesis. *Glob. Planet. Change* **242**, 104568. https://doi.org/10.1016/j.gloplacha.2024.104568 (2024).
2. May, A. & Crok, M. Carbon dioxide and a warming climate are not problems. *Am. J. Econ. Sociol.* **84**, 43–57 (2025).
3. Aouaini, F. et al. CO2 adsorption by molecular sieve 10A°, experimental and theoretical examination via statistical physics: modeling macroscopic and microscopic investigation. *Sep. Sci. Technol.* **57**, 2532–2542. https://doi.org/10.1080/01496395.2022.2080708 (2022).
4. Faisal, T. F., Chevalier, S. & Sassi, M. Experimental and Numerical Studies of Density Driven Natural Convection in Saturated Porous Media with Application to CO2 geological storage. *Energy Procedia* **37**, 5323–5330. https://doi.org/10.1016/j.egypro.2013.06.450 (2013).
5. Aouaini, F. et al. Study of the CO2 adsorption isotherms on El Hicha clay by statistical physics treatment: microscopic and macroscopic investigation. *Sep. Sci. Technol.* **54**, 2577–2588. https://doi.org/10.1080/01496395.2018.1548487 (2019).
6. Bouzgarrou, S. et al. Experimental Adsorption and Modelisation of CO_2 on Adsorbents Collected from Elborma Field in South Tunisia. *J. Surf. Eng. Mater. Adv. Technol.* **05**, 52–63. https://doi.org/10.4236/jsemat.2015.51006 (2015).
7. Bouzgarrou, S., Harzallah, H. S. & Slimi, K. Unsteady Double Diffusive Natural Convection in Porous Media-Application to CO2 Storage in Deep Saline Aquifer Reservoirs. *Energy Procedia* **36**, 756–765. https://doi.org/10.1016/j.egypro.2013.07.088 (2013).
8. Al-Ghurabi, E. H., Boumaza, M. M., Al-Masry, W. & Asif, M. Optimizing the synthesis of nanoporous activated carbon from date-palm waste for enhanced CO2 capture. *Sci. Rep.* **15**, 17132. https://doi.org/10.1038/s41598-025-00498-1 (2025).
9. Salamba, M. Q. et al. Porosity of Activated Carbon in Water Remediation: A Bibliometric Review and Overview of Research Perspectives. *ACS ES&T Water* **5**, 2070–2086. https://doi.org/10.1021/acsestwater.5c00100 (2025).
10. Yalçın, N. & Sevinç, V. Studies of the surface area and porosity of activated carbons prepared from rice husks. *Carbon N. Y.* **38**, 1943–1945. https://doi.org/10.1016/S0008-6223(00)00029-4 (2000).
11. Sanchez, J., NCharacterization of activated carbon produced from coffee residues by chemical and physical activationo Title. (2011).
12. De Oliveira, J. C. et al. No TitleRepresentative Pores: An Efficient Method to Characterize Activated Carbons. *Front. Chem.* https://doi.org/10.3389/fchem.2020.595230 (2021).
13. Al-Ghouti, M. A., Yousef, I., Ahmad, R., Ghrair, A. M. & Al-Maaitah, A. A. Characterization of diethyl ether adsorption on activated carbon using a novel adsorption refrigerator. *Chem. Eng. J.* **162**, 234–241. https://doi.org/10.1016/j.cej.2010.05.035 (2010).
14. Lee, J.-Y., Lee, B.-H., Chung, D.-C. & Kim, B.-J. CO2 Adsorption Behaviors of Biomass-Based Activated Carbons Prepared by a Microwave/Steam Activation Technique for Molecular Sieve. *Mater. (Basel)* https://doi.org/10.3390/ma16165625 (2023).
15. Michot, L. J. & Villiéras, F. Chapter 12.9 Surface Area and Porosity. In *Handbook of Clay Science* (eds Bergaya, F. et al.) 965–978 (Elsevier, 2006).
16. Jedli, H., Jbara, A., Hedfi, H. et al. A laboratory study of supercritical CO2 adsorption on cap rocks in the geological storage conditions. *Appl. Phys. A.* **123**, 254. https://doi.org/10.1007/s00339-017-0862-0 (2017).

17. Alabadi, A., Razzaque, S., Yang, Y., Chen, S. & Tan, B. Highly porous activated carbon materials from carbonized biomass with high CO2 capturing capacity. *Chem. Eng. J.* **281**, 606–612. https://doi.org/10.1016/j.cej.2015.06.032 (2015).
18. Lai, J. Y., Ngu, L. H., Hashim, S. S., Chew, J. J. & Sunarso, J. Review of oil palm-derived activated carbon for CO2 capture. *Carbon Lett.* **31**, 201–252. https://doi.org/10.1007/s42823-020-00206-1 (2021).
19. Raffah, B. M. et al. Morphological, sterical, and localized thermodynamics in the adsorption of CO2 by activated biocarbon from the white rot fungi Trametes gibbosa. *Sci. Total Environ.* **939**, 173326. https://doi.org/10.1016/j.scitotenv.2024.173326 (2024).
20. Fatima, S. S., Borhan, A., Ayoub, M. & Ghani, N. A. Modeling of CO2 Adsorption on Surface-Functionalized Rubber-Seed Shell Activated Carbon: Isotherm and Kinetic Analysis. *Processes* https://doi.org/10.3390/pr11102833 (2023).
21. Lu, T., Chen, Q. van der Waals potential: an important complement to molecular electrostatic potential in studying intermolecular interactions. *J. Mol.Model.***26**, 315. https://doi.org/10.1007/s00894-020-04577-0 (2020).
22. Bläker, C., Muthmann, J., Pasel, C. & Bathen, D. Characterization of Activated Carbon Adsorbents – State of the Art and Novel Approaches. *ChemBioEng Rev.* **6**, 119–138. https://doi.org/10.1002/cben.201900008 (2019).
23. Jedli, H., Bouzgarrou, S.M., Hassani, R. et al. CO2 adsorption onto activated carbon through functionalization by monoethanolamine: experimental and RSM modeling. *J. Therm. Anal. Calorim.* **150**, 7439–7449. https://doi.org/10.1007/s10973-025-14112-z (2025).
24. Kumar, A. & Jena, H. M. Preparation and characterization of high surface area activated carbon from Fox nut (Euryale ferox) shell by chemical activation with H3PO4. *Results Phys.* **6**, 651–658. https://doi.org/10.1016/j.rinp.2016.09.012 (2016).
25. Ugal, J. R., Mustafa, M. & Abdulhadi, A. A. Preparation of Zeolite Type 13X from Locally Available Raw Materials. *J. Chem. Pet. Eng.* **9**, 51–56. https://doi.org/10.1699/IJCPE.2008.1.8 (2008).
26. Almoneef, M. M., Jedli, H. & Mbarek, M. Experimental study of CO2 adsorption using activated carbon. *Mater. Res. Express* **8**, 65602. https://doi.org/10.1088/2053-1591/ac05fe (2021).
27. Pakseresht, S., Kazemeini, M. & Akbarnejad, M. M. Equilibrium isotherms for CO, CO2, CH4 and C2H4 on the 5A molecular sieve by a simple volumetric apparatus. *Sep. Purif. Technol.* **28**, 53–60. https://doi.org/10.1016/S1383-5866(02)00012-6 (2002).
28. Bouzid, M., Sellaoui, L., Khalfaoui, M., Belmabrouk, H. & Lamine, A. B. Adsorption of ethanol onto activated carbon: Modeling and consequent interpretations based on statistical physics treatment. *Phys. A Stat. Mech. its Appl.* **444**, 853–869. https://doi.org/10.1016/j.physa.2015.09.097 (2016).
29. Bouzid, M., Sellaoui, L., Rhouma, M. B. E. H., Bonilla-Petriciolet, A. & Lamine, A. B. Understanding the adsorption mechanism of carbon dioxide capture on hybrid zeolites prepared from rice husk ash via a modified statistical physics model. *Microporous Mesoporous Mater.* **381**, 113346. https://doi.org/10.1016/j.micromeso.2024.113346 (2025).
30. Nakbi, A., Bouzid, M., Ayachi, F., Bouaziz, N. & Ben Lamine, A. Quantitative characterization of sucrose taste by statistical physics modeling parameters using an analogy between an experimental physicochemical isotherm of sucrose adsorption on β-cyclodextrin and a putative biological sucrose adsorption from sucrose d. *J. Mol. Liq.* **298**, 111950. https://doi.org/10.1016/j.molliq.2019.111950 (2020).
31. Pang, X. et al. Theoretical study of indigotine blue dye adsorption on CoFe2O4/chitosan magnetic composite via analytical model. *Colloids Surfaces A Physicochem. Eng. Asp.* **589**, 124467. https://doi.org/10.1016/j.colsurfa.2020.124467 (2020).
32. Lamine, A. B. & Bouazra, Y. Application of Statistical Thermodynamics to the Olfaction Mechanism. *Chem. Senses* **22**, 67–75. https://doi.org/10.1093/chemse/22.1.67 (1997).
33. Missaoui, N. et al. Interpreting of the carbon dioxide adsorption on high surface area zeolitic imidazolate Framework-8 (ZIF-8) nanoparticles using a statistical physics model. *Microporous Mesoporous Mater.* **360**, 112711. https://doi.org/10.1016/j.micromeso.2023.112711 (2023).
34. Sghaier, W., Ben Torkia, Y., Bouzid, M. & Ben Lamine, A. CO2 adsorption investigation by statistical physics: Thermodynamic analysis for cooling cycle application. *J. Environ. Chem. Eng.* **9**, 105108. https://doi.org/10.1016/j.jece.2021.105108 (2021).
35. Raganati, F., Miccio, F. & Ammendola, P. Adsorption of Carbon Dioxide for Post-combustion Capture: A Review. *Energy Fuels* **35**, 12845–12868. https://doi.org/10.1021/acs.energyfuels.1c01618 (2021).
36. Mohamed, B., Qingyu, Z., Moggridge, D. G. & Abdelmottaleb, B. L. New insight in adsorption of pyridine on the two modified adsorbents types MN200 and MN500 by means of grand canonical ensemble. *J. Mol. Liq.* **263**, 413–421. https://doi.org/10.1016/j.molliq.2018.05.008 (2018).

Acknowledgements

The authors gratefully acknowledge the funding of the Deanship of Graduate Studies and Scientific Research, Jazan University, Saudi Arabia, through project number: (JU-202502103-DGSSR-ORA-2025).

Author contributions

Souhail. M Bouzgarrou: Conceptualization, Data curation, Investigation, Methodology, Validation, Visualization, writing—original draft, Writing–review & editing. Khouloud Guettiti, Amin Naifar: Supervision, Validation, Visualization; Fatma Aouaini, Rym Hassani, Gamal A. Abdelhamed Saad: Supervision, Validation, Visualization; Khouloud Guettiti, Amin Naifar, Afzal Husain Khan: Writing—review & editing.

Declarations

Competing interests

The authors declare no competing interests.

Additional information

Supplementary Information The online version contains supplementary material available at https://doi.org/10.1038/s41598-025-22526-w.

Correspondence and requests for materials should be addressed to S.B.

Reprints and permissions information is available at www.nature.com/reprints.

Publisher's note Springer Nature remains neutral with regard to jurisdictional claims in published maps and institutional affiliations.

Open Access This article is licensed under a Creative Commons Attribution-NonCommercial-NoDerivatives 4.0 International License, which permits any non-commercial use, sharing, distribution and reproduction in any medium or format, as long as you give appropriate credit to the original author(s) and the source, provide a link to the Creative Commons licence, and indicate if you modified the licensed material. You do not have permission under this licence to share adapted material derived from this article or parts of it. The images or other third party material in this article are included in the article's Creative Commons licence, unless indicated otherwise in a credit line to the material. If material is not included in the article's Creative Commons licence and your intended use is not permitted by statutory regulation or exceeds the permitted use, you will need to obtain permission directly from the copyright holder. To view a copy of this licence, visit http://creativecommons.org/licenses/by-nc-nd/4.0/.

© The Author(s) 2025